

Pre-Programmed Rod-Shaped Microgels to Create Multi-Directional Anisogels for 3D Tissue Engineering

Dominik L. Braunmiller, Susan Babu, David B. Gehlen, Maximilian Seuß, Tamás Haraszti, Andreas Falkenstein, Julian Eigen, Laura De Laporte,* and Jérôme J. Crassous*

Micron-scale anisometric microgels have received increasing attention to replace macromolecule solutions to create injectable 3D regenerative hydrogels. Interlinking these rod-shaped microgels results in microporous constructs, while incorporating magnetic nanoparticles inside the microgels enables their alignment to introduce directionality. This report demonstrates that the angle of microgel alignment in a static external magnetic field can be pre-programmed, broadening their applicability to artificially assemble into specific architectures. The magnetic rod-shaped polyethylene glycol microgels are prepared via in mold polymerization. Ellipsoidal maghemite nanoparticles, integrated as responsive fillers are pre-aligned either parallel or orthogonal to the long axis of the microgel with a weak magnetic field during rod fabrication to implement additional control over their magnetic orientation and allow their precise manipulation and actuation. The magnetic response of the microgels to static and rotating magnetic fields is discussed depending on various process and design parameters, such as magnetic field strength, angular frequency, and pre-alignment. Finally, the applicability of the approach for tissue engineering is highlighted by growing mouse fibroblasts in three dimensions within Anisogels, i. e., hydrogels containing a mixture of rods with both a parallel and orthogonal orientation, marking a new step toward more advanced functional cell templating for tissue engineering.


1. Introduction

Introducing magnetic properties into micron-scale building blocks is a way to introduce external control over different systems, ranging from micro-actuators possibly used in microfluidics,^[1] over soft robotics^[2] and implant development,^[3] to self-assembly for tissue engineering.^[4] In the field of tissue

engineering and regenerative medicine, an increasing focus has been laid on cultivating cells inside 3D scaffolds to stimulate and guide cell growth in a unidirectional manner. Many different functional tissues need unidirectional cell structures to sustain their functions^[5] for example cardiac cells for heart beat,^[6] cartilage either for reinforcement or reduced friction^[7] and nerve cells for axon growth.^[8] To support the formation of these unilateral structures, directional scaffolds can be used.^[9] Multiple approaches are possible to create such scaffolds, like using electrospun fibers,^[10] structured hydrogels,^[11] or introducing magnetic properties into hydrogels or anisometric microgels inside Anisogels.^[12] The use of magnetic fields enables spatial manipulation of material building blocks after injection, artificially recreating the aligned extracellular matrix (ECM) naturally surrounding the cells.^[10b,12,13] Microgels are often proposed to be self-assembled into scaffolds in a bottom-up manner.^[12a,14] They consist of nano- to micrometer sized cross-linked polymer networks with a wide range

of properties.^[15] Depending on the used monomers or precursor molecules, cross-linking density, or possible filler materials, microgels can be softer or stiffer,^[15] stimuli-responsive,^[12a,15,16] and more or less permeable.^[17] This diversity of controllable properties makes them an attractive choice for biotechnology applications, as they can be fine-tuned to deliver or capture certain molecules or mimic the cell environment.^[18]

D. L. Braunmiller, A. Falkenstein, J. Eigen, J. J. Crassous
Institute of Physical Chemistry
RWTH Aachen University
52074 Aachen, Germany
E-mail: crassous@pc.rwth-aachen.de

 The ORCID identification number(s) for the author(s) of this article can be found under <https://doi.org/10.1002/adfm.202202430>.

© 2022 The Authors. Advanced Functional Materials published by Wiley-VCH GmbH. This is an open access article under the terms of the Creative Commons Attribution License, which permits use, distribution and reproduction in any medium, provided the original work is properly cited.

DOI: 10.1002/adfm.202202430

S. Babu, D. B. Gehlen, M. Seuß, T. Haraszti, L. De Laporte
DWI – Leibniz-Institute for Interactive Materials
52074 Aachen, Germany
E-mail: delaporte@dwil.rwth-aachen.de

S. Babu, T. Haraszti, L. De Laporte
Institute for Technical and Macromolecular Chemistry
RWTH Aachen University
52074 Aachen, Germany

L. De Laporte
Advanced Materials for Biomedicine
Institute for Applied Medical Engineering
University Hospital RWTH Aachen
52074 Aachen, Germany

Previous works have already shown the use of microgel building blocks to grow cells inside,^[19] on the surface, or in between interlinked^[20] or magnetically aligned microgels.^[21] On one hand, the rod-shape of the microgels mimics the natural ECM filaments and allows for bigger and interconnected pores in the scaffold compared to materials consisting of spherical particles.^[13a,21,22] On the other hand, magnetically aligned rod-shaped microgels can be immobilized inside a surrounding hydrogel, resulting in linear fibroblast and nerve growth both *ex vivo*^[10b] and *in vivo*.^[13b] The microgels are prepared via an in-mold polymerization technique based on particles replication in a non-wetting template (PRINT) from polyethylene glycol (PEG) mixed with superparamagnetic iron oxide nanoparticles (SPION) as a reactive filler.^[12,13] As SPIONs are superparamagnetic nanoparticles with a rotatable magnetic moment, the anisometry of the microgel rods in combination with the interaction of the SPIONs allows for orientation of the rod-shaped microgels with their long axis along an external magnetic field, depending on their size and stiffness, the amount of embedded SPIONs, the magnetic field strength, and the viscosity of the surrounding fluid.^[13b] An additional advantage of these small microgels is their injectability, which enables bottom-up assembling after entering the body. However, so far, the applicability of this system is limited by the fact that microgel rods with SPION can only be oriented parallel to the magnetic field, while the design of more advanced tissues like cartilage^[7b,c] may require additional control over the orientation at different angles that could be achieved by mixing differently pre-programmed microgels. Therefore, microgels, for which their angle of alignment can be magnetically pre-programmed, can further provide new opportunities to hierarchically structure biomaterial systems.

In this study, ellipsoidal maghemite nanoparticles are employed to introduce variable magnetic properties into anisotropic magnetic microgels. α -Fe₂O₃ hematite spindles were first

converted into γ -Fe₂O₃ maghemite spindles with ferrimagnetic properties at room temperature with a fixed magnetic moment oriented along their long axis.^[23] Applying an external magnetic field onto these nanoparticles, they first align themselves along the magnetic field. At a sufficiently strong magnetic field, the nanoparticles further form dipolar chains.^[23] To integrate a specific magnetic moment into the microgels, the ellipsoidal nanoparticles are pre-aligned by applying a homogeneous magnetic field during the PRINT micro-fabrication of the microgels as summarized in **Figure 1**. Herein, we report that the orientation and response of the microgels to the magnetic field can be efficiently controlled depending on the pre-alignment conditions of the ellipsoidal maghemite nanoparticles. The integration of the nanoparticles was investigated via scanning electron microscopy (SEM). The dynamic magnetic response of the rod-shaped PRINT microgels was analyzed from their response to a rotating homogeneous magnetic field. Therefore, we adapted a bright field microscope with a custom-designed piezoelectric rotating stage fitted with circular Halbach arrays of different field strengths. Having demonstrated that the composite microgels could align either parallel or perpendicular to the applied field, their applicability for tissue engineering was further tested using both static and rotating magnetic fields. Hereby, the directional growth of fibroblasts within Anisogels is investigated, where 3D constructs containing mixture of pre-programmed microgels with a parallel and perpendicular orientation lead to cell alignment in both directions.

2. Results and Discussion

2.1. Ellipsoidal Maghemite Nanoparticles

The maghemite spindles used as anisotropic magnetic fillers are obtained from the conversion of silica-coated hematite

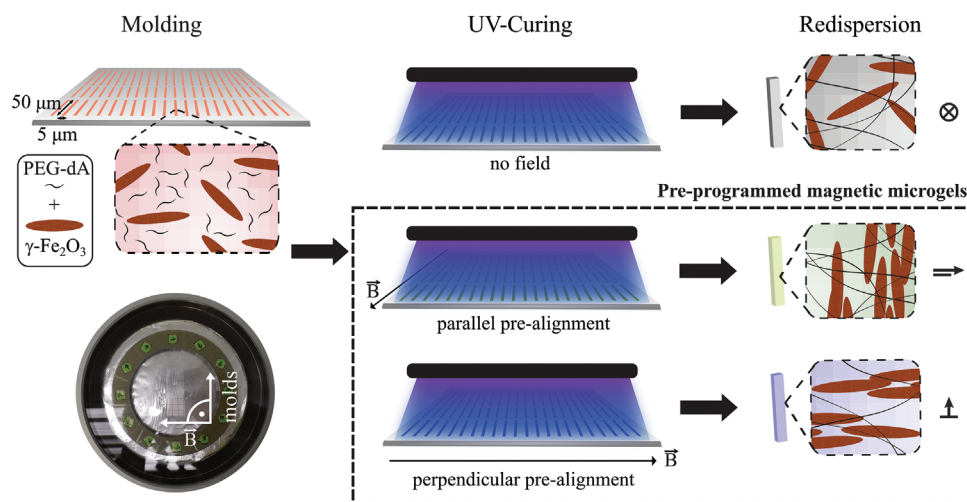


Figure 1. Fabrication of magnetic rod-shaped composite microgels via PRINT with different pre-alignment of the ellipsoidal nanoparticles. Step 1, Molding: PDMS molds with micron-scale cavities shown in the center of the photograph are filled with a dispersion containing PEG-DA, maghemite nanoparticles, and photoinitiator. Step 2, UV-Curing: The dispersion is then cured with UV in the absence or presence of a homogeneous magnetic field set by a Halbach array (see photograph) applied either parallel or perpendicular to the rod long axis. Step 3, Harvesting: Following the pre-alignment conditions, three distinct systems are obtained after harvesting the cured composite microgel rods: no field microgels, parallel and perpendicular pre-programmed microgels.

spindles into maghemite. The spindles are then redispersed by etching the silica shell under alkaline conditions. The synthesis of the particles, their conversion, and redispersion are detailed in the Figure S1 (Supporting Information). The initial characterization of the maghemite nanoparticles is carried out by various microscopy and scattering methods (Figure S2, Supporting Information). The average length of the nanoparticles determined from the statistical analysis of transmission electron microscopy (TEM) micrographs was determined at 260 ± 29 nm and the average diameter at 51 ± 6 nm. The stability of the maghemite aqueous dispersion was tested by dynamic light scattering (DLS) and the measured diffusion coefficient was compared to the expected value calculated based on the dimensions determined from the TEM analysis as proposed by Martchenko et al.^[24] The apparent isotropic diffusion of $3.65 \mu\text{m}^2 \text{s}^{-1}$ at 25°C (DLS) is in close match with the calculated value of $3.73 \mu\text{m}^2 \text{s}^{-1}$ asserting for the proper dispersion of the maghemite. In literature, the magnetic moment of the ellipsoidal maghemite nanoparticles is assumed to point along the long axis.^[23] It has been shown that comparable magnetite nanoparticles exhibit a strong magnetic response and can form highly ordered dipolar chains at low magnetic fields in the range of 150 mT.^[25] To determine the field dependence of the dipolar chain formation, SEM micrographs of the maghemite aqueous dispersion dried under a homogenous magnetic field were recorded. For the SEM measurements, samples of 0.1 wt.% nanoparticle solution were dried while exposed to a homogeneous magnetic field $B = 1$ mT set by an Halbach array as described in the Supporting Information.

This procedure was then repeated with $B = 10$ mT. As expected, the nanoparticles are increasingly self-assembling into dipolar chains with increasing field strength (Figure 2A–D). Even a weak field of 1 mT leads to some chain formation confirming the high magnetic response of the materials and the successful conversion from hematite to maghemite. For higher B , nearly all nanoparticles assemble into dipolar chains. At 10 mT, the nanoparticles inside the chains are mainly oriented parallel to the chain. In addition to the SEM measurements, a set of experiments in cross-polarization was conducted. In cross-polarization, the analyzer and polarizer are set up perpendicular to each other to ensure complete extinction of the light. Through this setup, only additionally polarized light is detected. The dipolar chains can polarize light depending on their orientation. When exposed to a rotating magnetic field of 68 mT, the dipolar chains, rotate with a rotation speed up to the maximal motor speed of 90 rpm (Video S1, Supporting Information). The chain sizes depend on B , the exposure time, and the angular frequency ω_{MF} (in the case of a rotating magnetic field). In addition, for the cross-polarization experiments, two Helmholtz coils were used to generate a quickly switchable homogeneous magnetic field and the linear polarizers were oriented to ensure a maximum intensity when the dipolar nanoparticle chains are aligned with the magnetic field. Switching on the magnetic field leads to an increase in intensity if dipolar chains are formed. These experiments were conducted with weak magnetic fields between 0 and 4.5 mT and show that chain formation already occurs around 0.5 mT.

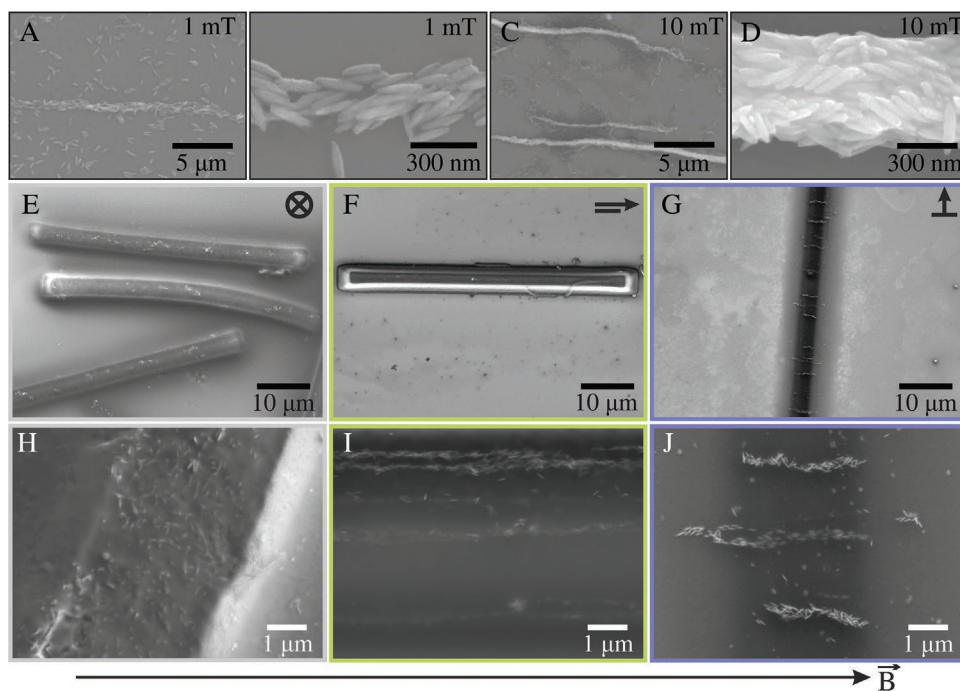


Figure 2. SEM micrographs (secondary electron) of ellipsoidal maghemite nanoparticles aqueous dispersions dried under a homogeneous magnetic field of A,B) 1 mT and C,D) 10 mT. E–J) SEM micrographs of microgel rods with incorporated ellipsoidal maghemite nanoparticles. E,H) In the absence of magnetic pre-alignment, the nanoparticles are randomly distributed inside the microgels. The microgel rods with maghemites pre-aligned with a 10 mT magnetic field exhibit dipolar chains oriented either F,I) parallel or G,J) perpendicular to the microgel rod long axis depending on the synthesis conditions.

2.2. Preparation and Characterization of the Magnetic Microgel Rods via PRINT

The rod-shaped magnetic microgels are produced using PRINT as schematically summarized in Figure 1 and described in more detail in the Supporting Information. A template containing $5 \times 5 \times 50 \mu\text{m}^3$ cavities is filled with a precursor solution containing the ellipsoidal maghemite nanoparticles. While applying a magnetic field of 10 mT on the template using a Halbach array, the PEG polymer chains are UV-cross-linked in a nitrogen atmosphere for 1 h. The direction of the magnetic field is set depending on the preferred alignment of the nanoparticles. For samples without pre-alignment, ellipsoidal nanoparticles are incorporated but no field is applied during UV-Curing. The nanoparticle content of the microgels, determined by the ratio of the maghemite content to polyethylene glycol diacrylate (PEG-DA), is 1.6 wt.%. SEM measurements were first conducted to ensure the successful incorporation of the maghemite anisotropic magnetic fillers into the PRINT microgels. Micrographs of composite rod-shaped microgels cured under an applied magnetic field (Figure 2A–D) indicate that a weak magnetic field with a strength of 10 mT leads to dipolar chain formation in the direction of the magnetic field. Dipolar chains close to the surface can be seen in SEM measurements of the rod-shaped microgels (Figure 2E–J). Inside microgel rods prepared without a magnetic field (Figure 2E,H), the nanoparticles are randomly distributed within the polymer

network. A parallel field orientation to the long axis of the molds leads to dipolar chains following the entire length of the microgels (Figure 2F,I). The perpendicular pre-alignment result in shorter chains perpendicular to the main axis (Figure 2G,J). The magnetic moment of the prepared microgel rods corresponds to the direction of the alignment of the dipolar chains. As these images were taken after removal of the magnet, it confirms that the ellipsoidal maghemite nanoparticles and their assemblies into dipolar chains are fully integrated inside the cross-linked microgels.

2.3. Static Control

The incorporation of ellipsoidal maghemite nanoparticles allows us to add variable magnetic properties to the microgels. Previous magnetic rod-shaped microgels with SPIONs as magnetic fillers only orient in one direction to the magnetic field,^[12,13] while the ellipsoidal nanoparticles enable the pre-programming of different orientations to the field (Figure 3). The dipolar chains formed by the maghemite nanoparticles aligned along the magnetic field during PRINT fabrication are fixed due to microgel crosslinking. Through this pre-alignment, the magnetic moment of the microgels can be pre-programmed. Without applying a magnetic pre-alignment during the PRINT synthesis (Figure 3A), the microgel rods exhibit a random orientation to the applied static external

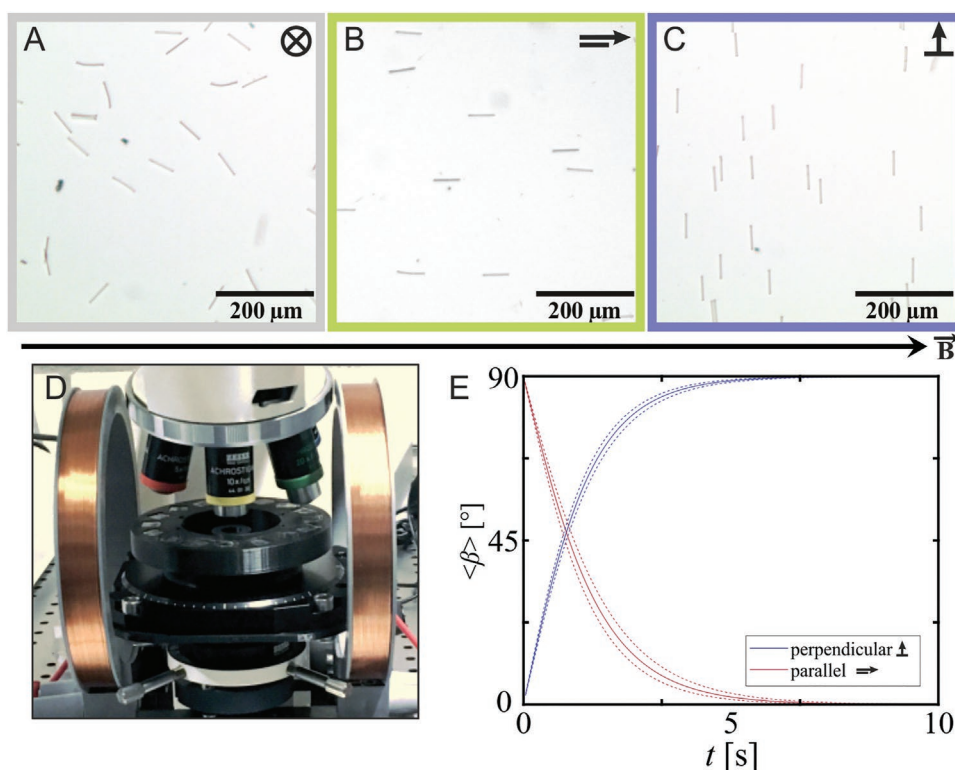


Figure 3. A–C) Magnetic microgel rods under a static horizontal magnetic field of 68 mT. The pre-alignment of the nanoparticles determines the orientation of the rods. Without pre-alignment, there is no uniform orientation. D) Experimental setup for experiments with magnetic fields consisting of a bright-field microscope equipped with a rotating stage holding a Halbach array. Alternatively, the Helmholtz coils can be employed for the application of weak static magnetic fields. E) Relaxation of the magnetic microgels after a quick rotation of the magnetic field by 90°. Displayed are mean curves derived from the relaxation curves of multiple microgels. The dashed lines indicate the standard errors.

magnetic field (further discussed in Section 2.4). The microgels containing maghemite nanoparticles pre-aligned parallel to the long axis of the microgel, orient themselves parallel to the magnetic field (Figure 3B), whereas a perpendicular pre-alignment leads to perpendicular microgel orientation (Figure 3C). Following these results, we expect that any angle of alignment could be pre-programmed during the PRINT synthesis.

Under a magnetic field of 10 mT, SPIONs form strings aligned along the magnetic field lines, comparable to the dipolar chains formed by ellipsoidal maghemite nanoparticles. To compare their effect on microgel orientation, and as a reference sample, rod-shaped microgels, with the same mass content of SPIONs, are prepared using the same procedure with a parallel and a perpendicular oriented as well as without a magnetic field. All of these microgels align along the magnetic field, as described in previous publications for microgel rods prepared without a magnetic field.^[12,13] Thus, in contrast to the ellipsoidal maghemite nanoparticles, no pre-programming of the microgels can be achieved by incorporating the SPIONs (Figure S4, Supporting Information for more details).

2.4. Dynamic Control

Additionally, to the static control of the orientation of the microgels, we can control the response of the rod-shaped microgels to a dynamic field. Considering a ferromagnetic rod immersed in a Newtonian liquid subjected to a rotating magnetic field, the rotation of the particle is determined by the exerted viscous and magnetic torques. For a magnetic field B with a magnetic moment m rotating at a constant angular frequency ω_{MF} , the corresponding equation of motion is the following^[26]

$$\gamma \left(\omega_{MF} - \frac{d\theta}{dt} \right) = mB \times \sin \theta \quad (1)$$

where γ corresponds to the rotational drag coefficient and θ describes the angle between the direction of the magnetic field and the magnetic moment of the rod. When the magnetic torque dominates, the magnetic field and the rod rotate synchronously and θ remains constant. When the viscous torque dominates, θ changes periodically and the rod tumbles. The transition between the synchronous and asynchronous regimes is determined by the critical angular frequency ω_c defined as^[26]

$$\omega_c = \frac{m \times B}{\gamma} \quad (2)$$

ω_c increases with the magnetic moment m of the microgels and the magnetic field strength B , and is reduced for higher drag forces (drag coefficient γ). To characterize the magnetic response of the microgel rods, we performed different analyses under a dynamic magnetic field. At first, the microgel rods were oriented under a static magnetic field (68 mT) and consecutively forced to re-orient by swiftly changing the direction of the field by 90° at 90 rpm. The microgels change their orientation in response to the changed orientation of the magnetic field. On average, the microgels with pre-aligned maghemite nanoparticles inside change their orientation within

2–7 s (Figure S3, Supporting Information). The perpendicular pre-alignment leads to a slightly faster relaxation than the parallel one but most of the microgels of both batches re-orient within this period. Furthermore, it should be noted that neither before nor after the field shift are all of the rods perfectly oriented along the magnetic field, but are varying by a few degrees around the field directions. This also applied to both pre-alignment directions. The angular change of circa 30 microgels per batch was tracked. Depending on the pre-alignment, the orientation of the microgel rods defined by the angle $\beta(t)$ varies from 0 to 90° (parallel) or 90° to 0° (perpendicular). Using Equations 1 and 2, we derived the following equations for the relaxation experiments:

A) 90° to 0° (perpendicular pre-alignment):

$$\beta(t) = 2 \times \arctan(e^{-\omega_c \times t}) \quad (3)$$

B) 0° to 90° (parallel pre-alignment):

$$\beta(t) = \frac{\pi}{2} 2 \times \arctan(e^{-\omega_c \times t}) \quad (4)$$

The response of the individual microgels was fitted by Equations 3 and 4 as shown in Figure S3 (Supporting Information). The mean value of ω_c determined from this analysis was 0.80 ± 0.08 and 0.91 ± 0.05 rad s⁻¹ for the parallel and perpendicular pre-alignment, respectively. The resulting relaxation curves using the average ω_c and Equations 3 and 4 are shown in Figure 3E. Microgels without pre-aligned maghemite nanoparticles show no significant orientation change during this experiment, only a small angular change in the direction of the rotating magnetic field was observed. As shown in Figure 3A, these rods do not orient uniformly under a static magnetic field, this small rotational movement indicates that the rods still have a weak response to a changing rotating field. The relaxation experiments were also conducted on microgels with incorporated randomly distributed SPIONs. These show a slower relaxation process than pre-aligned maghemite microgels and have a mean ω_c of 0.40 ± 0.06 rad s⁻¹ (Figure S5, Supporting Information for further detail on the analysis).

To determine the magnetization and the critical rotation frequency of the different magnetic microgels, experiments with a continuously rotating magnetic field were performed. ω_c is the limit of the synchronous rotation regime, in which the rotation of motor and rod are synchronous but slightly offset.^[26,27] Above ω_c , in the asynchronous regime, the rods still show a rotational movement over long times but due to the fast motor rotation frequency, they start to tumble (Video S2, Supporting Information). The synchronous rotation of the microgels is interrupted by a backward movement until the orientation of the pre-aligned maghemite chains corresponds again with the orientation of the magnetic field. This results in an oscillating movement around the mean angular frequency. For the asynchronous regime, the cumulative angle change $\phi(t)$ (Figure 4A) shows oscillations with an increasing periodicity at higher ω_{MF} . When the microgel rotation frequency ω increases in the synchronous regime with an increasing field rotation frequency ω_{MF} , for $\omega_{MF} > \omega_c$, ω decreases due to increasing tumbling.

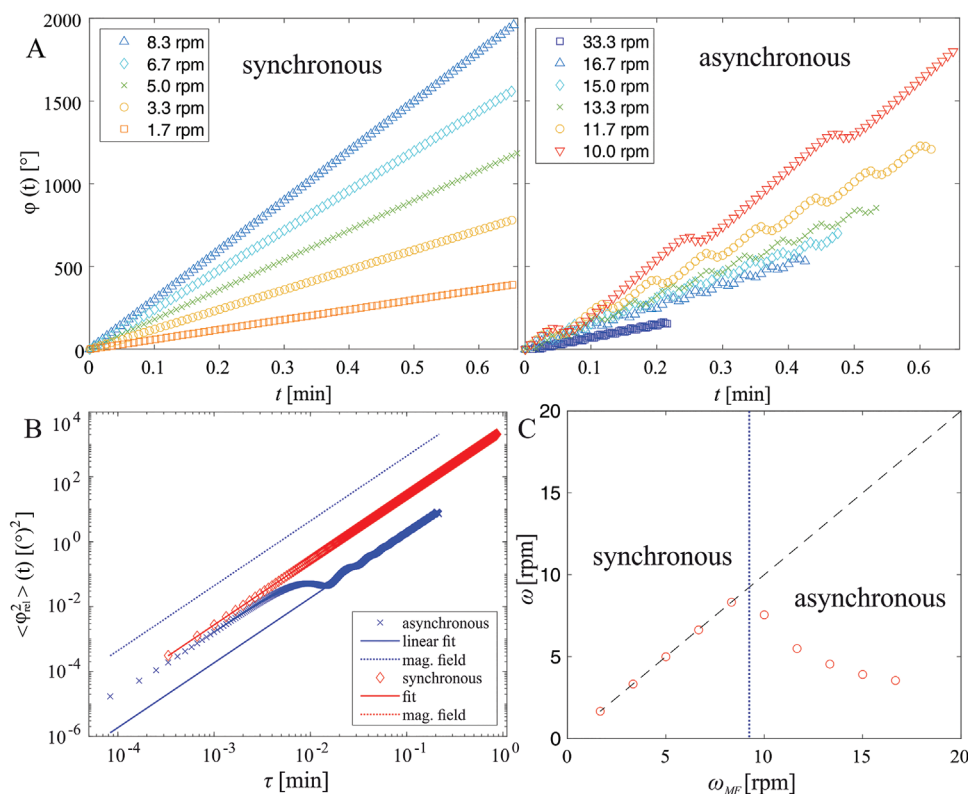


Figure 4. A) Cumulative angular displacement measured on a microgel with parallel magnetic pre-alignment at different field rotation frequencies ω_{MF} with a field of 68 mT within the synchronous (left) and asynchronous (right) regimes. B) An exemplary plot of the mean angular displacement for a rod rotating synchronously (red circles) and asynchronously (blue crosses). The solid lines correspond to the long-time average rotation frequency ω , while the dotted lines represent ω_{MF} . C) An exemplary plot of the dependence of ω on ω_{MF} (red circles) determined on one single microgel rod at 68 mT. Two rotation regimes can be identified: a synchronous rotation with $\omega = \omega_{MF}$ (dashed line) with a transition to an asynchronous rotation with $\omega < \omega_{MF}$ above ω_c (dotted line).

The long-time microgel rotation frequency ω can be calculated from the mean squared angular displacement $\langle \Delta\phi^2 \rangle(\tau)$ for the synchronous and the asynchronous regime defined as

$$\langle \Delta\phi^2 \rangle(\tau) = \langle |\phi(t) - \phi(t - \tau)|^2 \rangle \quad (5)$$

where τ refers to a certain time interval. Synchronous rotation of the microgel rods and the magnetic field orientation results in a linear dependence of $\langle \Delta\phi^2 \rangle(\tau)$ against τ^2 (Figure 4B). In the asynchronous regime, the periodicity of the tumbling motion correlates to the oscillation around the long-time rotation frequency of the microgels, represented by the dependence $\langle \Delta\phi^2 \rangle(\tau) = \omega^2 \tau^2$ at large τ in Figure 4B (solid line). The fits in both regimes consider primarily the longer τ for the determination of ω . While ω_{MF} (Figure 4B, dotted lines) matches ω in the synchronous rotation regime, it deviates above the critical rotation frequency ω_c , which is experimentally determined from the deviation between ω_{MF} and ω (Figure 4C, dotted line).

To determine the critical rotation frequency and the influence of the pre-alignment, multiple experiments were conducted for the three different microgel types at different B and ω_{MF} . The microgel rotation frequencies were determined with the method described above and by averaging more than 30 rods for each data point. Dependent on the pre-alignment, the microgel rods respond differently. As established above,

the microgels without a pre-alignment of the maghemite nanoparticles do not have a uniform orientation to a static magnetic field and only a minimal angular change when the magnet is quickly rotated by 90° . Interestingly, in a continuously rotating magnetic field, they can rotate with the field (Figure 5A) but the different rods do not have a uniform orientation to the magnetic field and the resulting rotation frequency does not depend on their orientation relative to the magnetic field. This corresponds to the absence of a fixed magnetic moment. The rotation frequency ω of the microgels increases with increasing ω_{MF} and B . Although the rods do not show tumbling as an indication of the asynchronous regime, only rotation frequencies up to 1 rpm can be achieved when $\omega_{MF} > 1$ rpm for $B = 68$ mT. A more detailed understanding of the mechanisms has yet to be achieved. Similar to these results, an applied magnetic field strength of 6 to 36 mT leads to a maximum angular frequency of 0.1 rpm and 0.9 rpm, respectively. While there is a larger difference between 6 and 36 mT, the magnetic response is almost the same for 36 and 68 mT. This might indicate a magnetic saturation of the microgels at these field strengths.

For microgel rods with a parallel pre-alignment, the magnetic response is significantly stronger than without a pre-alignment. The microgel rods show a synchronous or asynchronous rotation depending on ω_{MF} and B . For 36 and 68 mT, the rods mostly rotate synchronously up to 5 rpm (0.5 rad s^{-1}), which

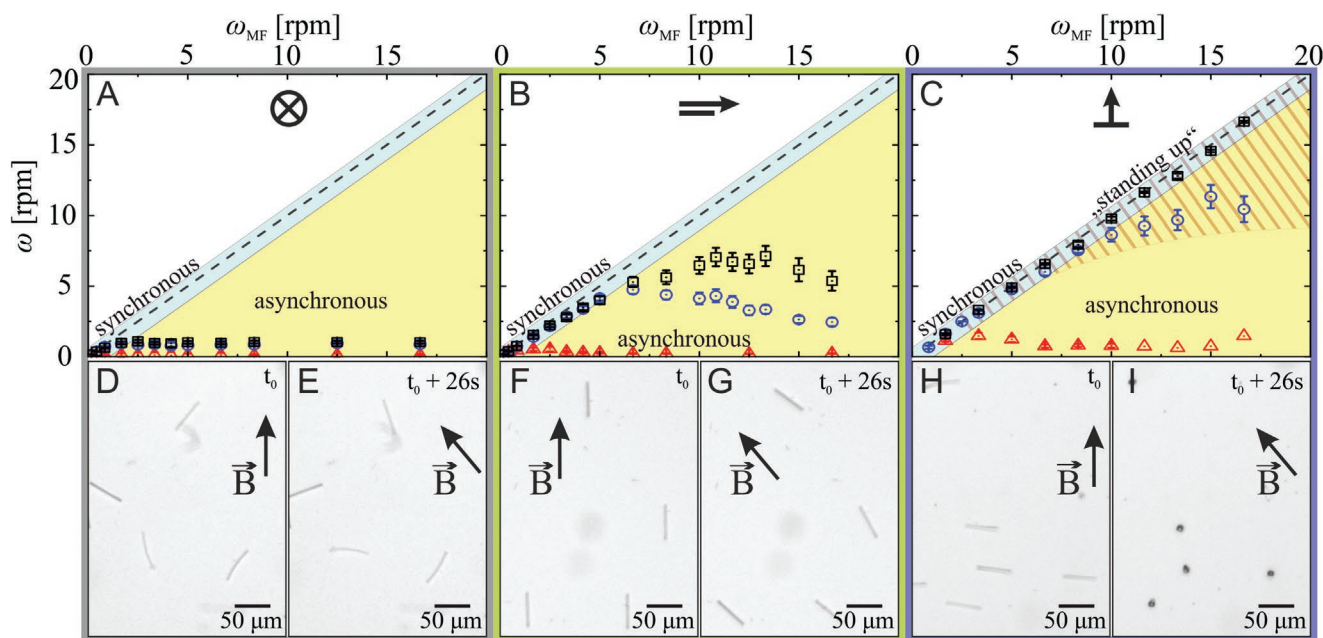


Figure 5. Resulting mean rotation frequencies ω of magnetic rod-shaped microgels determined for $B = 6$ mT (triangles), 36 mT (circles), and 68 mT (squares) for microgels without pre-alignment A), parallel pre-alignment B) and perpendicular pre-alignment C) of the maghemite nanoparticles. Depending on the pre-alignment conditions, different rotation regimes can be observed at the different magnetic field strength B and rotation frequency ω_{MF} , i. e., the synchronous (blue areas) and asynchronous (yellow areas) regimes and an additional “standing up” regime in C) resulting from the dynamic reorientation orthogonal to the surface (hatched areas) starting at 3–4 rpm. D–I) Timestep snapshots of the different microgels, showing the non-uniform rotation (68 mT, 7 rpm; D,E) of microgels without pre-alignment, the uniform synchronous rotation with parallel pre-alignment (68 mT, 7 rpm; F,G), and the “standing up” of rods with perpendicular pre-alignment (68 mT, 15 rpm; H,I).

is in reasonable agreement with the relaxation experiments ($\omega_c = 0.8 \text{ rad s}^{-1}$). With increasing ω_{MF} , the number of rods showing an asynchronous regime and the difference between ω and ω_{MF} increases. The influence of the field strength on the rotation frequency seems to be stronger in the asynchronous regime, as the rotation frequencies for 36 mT decrease faster with increasing ω_{MF} . For both field strength, ω_c is in the order of 5–6 rpm, whereas for $B = 6$ mT, it is lower than 1 rpm. The fact that ω_c is comparable at higher B is pointing once again to the saturation of the magnetic response. ω_c for 68 mT is significantly lower than with the relaxation experiments, since the relaxation experiments are not conducted close to the glass and thus exhibit weaker frictional forces.

Rods with a perpendicular pre-alignment show a similar behavior up to $\omega_{MF} \approx 2$ rpm at the difference that for $B = 6$ mT, the rods exhibit a stronger magnetic response than microgel rods with a parallel pre-alignment in agreement with our former observations on the relaxation experiments. At this field strength, the rods then start to rotate asynchronously. However, at higher B and ω_{MF} we observe that the microgel rods start to “stand up” (see Videos S3 and S4, Supporting Information). Indeed, conversely to rods with a parallel pre-alignment that can only align the magnetic moment when laying along the field, rods with a perpendicular pre-alignment only need to have their long axis perpendicular to the field. When deposited at the surface of the glass, it then results in the observed perpendicular alignment within the imaging plane under a static field. Upright rod rotating around the long axis exhibits a lower frictional torque as when they lay at the glass,

which is one of the driving forces for them to stand-up. The same observation was made when letting the rods sediments under a rotating magnetic field. It is interesting to note that such dynamic orientation behavior was already observed for hematite spindles having a magnetic moment with their basal plane, when subjected to a high-frequency alternating field.^[28] Why they do stand up from a flat conformation at the glass is still unclear and is the consequence of unbalanced forces exerted on the rotating rods. The latter may be related to hydrodynamic interactions with the surface of the glass and to the slight bending of the rods. For $B = 68$ mT the rods rotate synchronously on the whole range of applied ω_{MF} with a transition from a planar rotation to an upwards rotation starting around 3–4 rpm, whereas, for $B = 36$ mT, a coexistence between a synchronous upward rotation and asynchronous planar rotation is observed at higher ω_{MF} . These results illustrate the importance of the pre-alignment conditions to control dynamically the orientation of the microgel rods in the third dimension offering extra control on their possible alignment.

2.5. Cellular Alignment in Anisogels

To explore the potential of these pre-aligned microgel rods in tissue engineering, Anisogels (soft hydrogels loaded with microgel particles) were prepared using microgels with maghemite particles aligned in parallel or perpendicular directions to the microgel long axis as described in the Experimental Section and in more detail in the Supporting Information. To

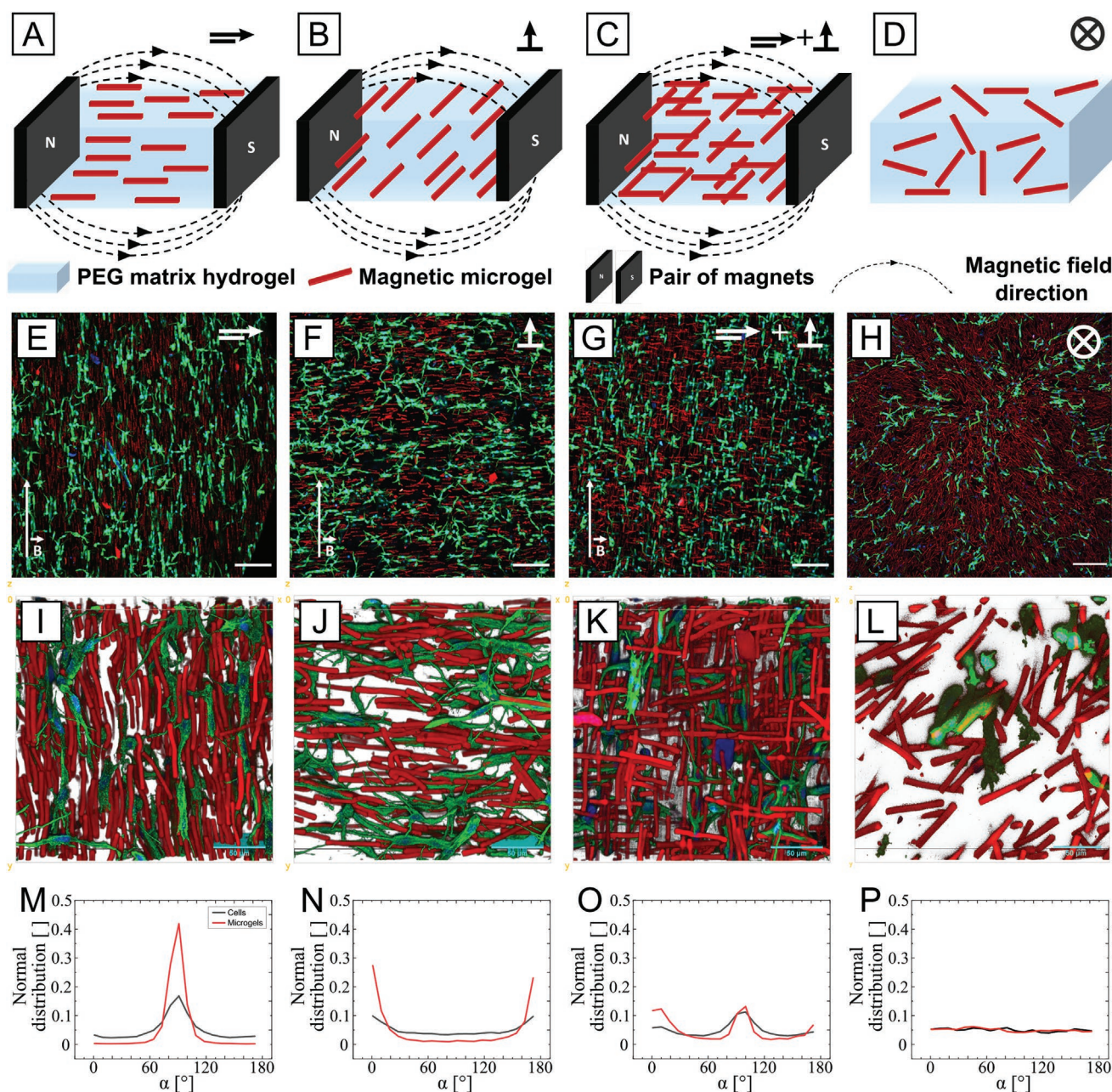


Figure 6. A–D) Schematics of Anisogels containing microgels pre-aligned in A) parallel, B) perpendicular, C) a combination of parallel and perpendicular directions, and D) a control hydrogel with randomly distributed microgels. E–H) Confocal images of mouse fibroblast cells after four days of culture in the above Anisogel conditions. At least 4 samples were imaged per condition. Scale bar = 200 μm . I–L) 3D reconstructions of 50 μm thick stacks of the respective culture conditions recorded at higher magnification. Scale bars = 50 μm . M–P) Plots of normalized angle distributions of cells and microgels in the different conditions respectively, which are proving that the cells grow in a direction(s) determined by the orientation of microgels present in the Anisogels. The black and red lines refer to the orientation and the cells and microgels, respectively.

prevent iron-cytotoxicity a low concentration of nanoparticles is used inside each microgel and the microgel content inside the Anisogels is only 1–2 vol.%. Considering the precursor solution concentration in maghemite of 3.6 mg mL^{-1} the maximum iron concentration is in the order of 72 $\mu\text{g mL}^{-1}$ for which a low cytotoxicity is expected.^[29]

Fibroblast cells were cultured in these Anisogels containing either parallelly or perpendicularly pre-programmed

microgels or a combination of these two in equal amounts. As a control, cells were cultured in an Anisogel containing 2 vol.% of randomly oriented microgels in the absence of applied magnetic field. At least four samples were made for each condition and cell growth was observed after 4 days with confocal microscopy (Figure 6). For this purpose, fluorescently labelled microgels (red) were synthesized and the cell nucleus (blue) and actin filaments (green) were labelled as described

in the Supporting Information. Figure 6E–H present 2D low magnification micrographs recorded for the different preparations, while Figure 6I–L represent the corresponding 3D reconstructions acquired at higher magnification (Videos S5–S8, Supporting Information for the original *z*-stacks). A closer look at the 3D reconstructions clearly confirmed that the microgels maintain their orientation within the Anisogels during the time of the culture (Figure 6I–L).

The cells grew well in all four cases and upon analyzing the orientation of cells in each preparation from the low magnification micrographs, it was observed that they grew in directions following the microgel orientation. This is further verified by the orientation analysis of both microgels and cells, shown in Figure 6M–P (see Supporting Information for further detail on the analysis). The cells are able to sense the anisotropy and align themselves along the direction of microgels as opposed to the scenario in control samples (Figure 6H,L), where the cells grow without any directionality (Figure 6P). It is also interesting to see that the randomly aligned microgels do not hinder cell growth, but instead allow cells to grow in all directions similar to the control condition in the absence of microgels (Figure S6, Supporting Information), proving once again the importance of microgel alignment to trigger an anisotropic cell response.

In an additional experiment, mouse fibroblasts were cultivated under comparable experimental conditions to check for fibrosis. No extensive production of collagen I was detected confirming the absence of significant fibrosis in the system (Figure S7, Supporting Information).

The Anisogels with the parallel pre-alignment (Figure 6A,E) are characterized by a narrow distribution of their orientation (Figure 6I), the same holds for the cells, which follow the microgels direction. In the case of the perpendicular alignment (Figure 6B,F), the alignment of both microgels and cells seems less pronounced (Figure 6J). Indeed, these microgels could still rotate around their short axis during crosslinking of the surrounding gel of the Anisogel, keeping their magnetic moment aligned to the field (Figure S8, Supporting Information). Cells seem sensitive to this effect and although they follow the orientation of the microgels, their orientation is less defined. The fact that most microgels appear to be mainly aligned parallel to the surface may be related to the influence of the substrate and the fact that the confocal micrographs are recorded 20 μm above the glass substrate. This additional degree of alignment can be considered as an asset as it could allow to extend upon the classical unidirectional cell growth observed in former Anisogels to planar growth. In the case where both parallelly and perpendicularly pre-programmed microgels are present (Figure 6C,G,K), cell growth is not hindered by the presence of microgels in the orthogonal direction but rather the growth is dominated in the two directions (Figure 6O). This indicates the ability of cells to detect and respond to multiple directional cues in the same system, which could be beneficial in designing even more complex tissue engineered constructs.

Finally, instead of simply applying a static magnetic field to the microgels during the enzymatic crosslinking of the hydrogel, a 50/50 mixture of perpendicularly and parallel pre-aligned microgels (1 vol.%) was first subjected to a rotating magnetic field (70 mT, 10 rpm) for 4 min followed by a static field for another 6 minutes during the gelation process as

described in more detail in the Experimental Section and in Figure 7A. Note that for these experiments the activated enzyme Factor XIII concentration was reduced to slow down the gelation kinetics, which was here completed within 10 min. Due to the rotation of the magnetic field the perpendicularly pre-aligned microgels “stood up” pointing to the *z*-direction while the parallel microgels rotated in the *xy*-plane. After 4 min the rotation of the magnetic field was stopped to allow the parallel pre-aligned microgels to orientate along the field, while the perpendicularly pre-aligned microgels should maintain their upright configuration until the Anisogel was fully crosslinked after 10 min. This Anisogels were further employed for cell culture for 4 days and imaged via confocal microscopy as shown in Figure 7C,D. While not all perpendicularly pre-aligned rods are perfectly upright, the two microgel orientations are clearly visible. It could also be seen that the cells grew in both directions demonstrating the potential of our approach to create a 3D scaffold using a dynamic orientation control of the perpendicularly pre-aligned microgels and to realize assembly that could not be achieved with a simple static field. The 3D projection of the image stack can be found in the Video S9 (Supporting Information). A more systematic investigation of the microgel alignment during the gelation is currently necessary for the optimization of the process. In the future, a combination with 3D printing is envisioned for the creation of scaffolds able to recreate complex structures such as cartilage for which an upright configuration at the bottom and a planar

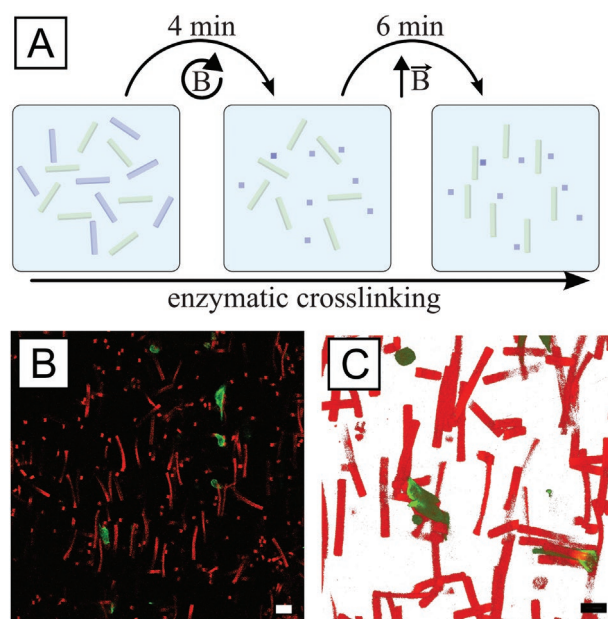


Figure 7. A) Schematics of the orientation of the microgel rods during the preparation of mixed Anisogels under application of a rotating field (70 mT, 10 rpm) for 4 min leading to upright perpendicularly pre-aligned microgels (blue) and the subsequent orientation of the microgels with a parallel pre-alignment (green) along the field after the engine was stopped for 6 min until the end of the gelation. B) Confocal micrograph of the Anisogel after cell culture showing microgels alignment in the *y*- and *z*-directions (red) and the directional growth of fibroblasts (green). C) 3D reconstruction of a 50 μm thick stacks recorded at a higher magnification. Scale bars = 30 μm .

configuration at the top are desired. In vivo experiments have already demonstrated the in vivo applications of the Anisogels for spinal cord injuries in respect to their low cytotoxicity and fast gelation preventing dilution of the materials by body fluids.^[13b] The high magnetic susceptibility of the presented microgels allows their alignment at low magnetic field that could be generated with electromagnets or Helmholtz coils.

3. Conclusion

Having a high level of spatial control over biomaterial building blocks is crucial for building complex 3D scaffolds via a bottom-up approach. This study demonstrates that we can successfully incorporate ellipsoidal ferromagnetic maghemite nanoparticles in a pre-aligned direction during PRINT. The pre-alignment enables us to pre-program the angle of orientation of anisometric magnetic microgels inside a static magnetic field and thus to obtain microgels with a defined magnetic dipole. In contrast, previous rod-shaped microgels using paramagnetic SPIONs as magnetic fillers, only orient parallel to the field lines, with or without SPION pre-alignment. Incorporating and pre-aligning ellipsoidal maghemite nanoparticles instead provide a higher degree of control over the orientation of the resulting magnetic microgel rods, depending on the predefined magnetic dipole orientation. Furthermore, the resulting microgels respond faster to a shifting magnetic field compared to SPION loaded microgels at similar nanoparticle concentration. Besides the static control of the orientation, we could demonstrate that the orientation can be altered dynamically by applying a rotating magnetic field, thereby extending the 2D orientation to the third dimension. The presented magnetic rotational spectroscopy experiment provides a powerful tool to test the adhesive properties of the microgels with different substrates. Further on, the strategy developed for the synthesis of these ferromagnetic microgels can be extended to different materials, shapes, and sizes for the design of multi-responsive actuators, devices, and swimmers at the microscale bearing some potential for the design of therapeutic microbots for non-invasive surgical interventions.^[30]

For tissue engineering, mixtures of microgels with different polarizations were added inside an Anisogel, creating alignment in both parallel and perpendicular directions using without hindering each other using both a static and dynamic orientation control. This led to cell alignment in both directions and opens the opportunity to orthogonally study multiple biochemicals, mechanical, and physical guiding cues in different directions and potentially selectively influence the growth of different cell types in co-culture. More especially, the static and dynamic control in combination with 3D printing may offer the possibility to easily prototype complex scaffolds with a stratified structure for functional tissue engineering.

4. Experimental Section

This experimental section represents a condensed overview over the main methods used in this paper. More details can be found in the Supporting Information.

Preparation of Magnetic Rod-Shaped Microgels: The rod-shaped magnetic microgels were produced using particle replication in a non-wetting template (PRINT, Figure 1). A precursor solution, consisting of 20 μL PEG-DA (700 Da) with a photoinitiator (Irgacure D 2959, 1 mol.%), a fluorescent dye (Methacryloxyethyl thiocarbonyl rhodamine B, 0.5 wt.%) and 80 μL of ellipsoidal maghemite nanoparticles dispersed in PEG-OH (200 Da, 4.5 mg mL⁻¹), was put onto a polydimethylsiloxane (PDMS) template containing $5 \times 5 \times 50 \mu\text{m}^3$ molds and applied with polyethylene terephthalate (PET) film. The total concentration of PEG-DA in the precursor solution was 20 wt %. Through careful lifting of this film, the excess of the precursor solution was removed. The PEG-DA polymer chains were UV-cross-linked in a nitrogen atmosphere for 1 h. A 254 nm UV light was used at an intensity of 2.6 mW cm⁻² for the microgel cross-linking. During this period, a magnetic field of 10 mT was applied to the template using a Halbach array to pre-align the maghemite nanoparticles. The direction of the magnetic field was changed depending on the preferred alignment of the nanoparticles. For samples without pre-alignment, ellipsoidal nanoparticles were mixed into the precursor solution, but no field was applied. To harvest the microgel rods, a water-soluble poly(vinylpyrrolidone) adhesive was used to glue the PDMS molds with microgels to a glass slide, after which they were dried for four days at room temperature. Afterward, the microgel rods were removed from the glass slide after washing with water and purified through centrifugation and redispersion in water. The nanoparticle content of the microgels, determined by the ratio of maghemite to PEG-DA, was around 1.6 wt.%.

Scanning Electron Microscopy: The samples were prepared by drying 20 μL of the batch on freshly cleaned silica wafers at room conditions. The wafers were sonicated for 15 min in isopropanol and plasma cleaned in air plasma for 15 min afterward. For investigations of the influence of a magnetic field, the drying process was conducted inside of differently strong Halbach arrays. SEM measurements were performed using a JSM-7800F field emission scanning electron microscope (Jeol) for secondary electron (SE) micrographs and backscatter detector (BSD) micrographs. Acceleration voltages used varied from 5–15 keV depending on desired penetration depth.

Magnetic Response Experiments: To study the magnetic response of the magnetic microgels a Zeiss AxioScope modified with a rotational stage driven by a piezoelectric engine PILine U651.03 (Figure 3D) was used. The magnetic field was applied by circular Halbach arrays consisting of different numbers and sizes of neodymium magnets. They can be mounted onto the stage to apply rotating or oscillating magnetic fields of different field strengths (1–68 mT) and different rotations frequencies (0.1–90 rpm). The microscope can also be fitted with two Helmholtz Coils creating a weak, static homogenous field of 0 to 5 mT. For the experiments in cross-polarization, two linear polarizers were mounted before and after the sample with a 90° offset to ensure complete extinction of the transmitted light.

The experiments on dynamic control over the microgel rods were performed with the above-described magnetic setup. Thereby glass slides were cleaned with isopropanol in an ultrasonic bath for 15 min and treated with air plasma for 15 min. The sample was sealed in with Secure-Seal spacers with wells of a diameter of 9 mm and a height of 0.12 mm. For the 90° shift experiments the samples were directly placed inside the center of a Halbach array and thereby the microgel rods were oriented without letting them sediment to the glass surface. Consecutively, the magnetic field direction was changed by rotating the stage by 90° with a speed of 90 rpm. The microgels were recorded while re-orienting to the new field direction.

For experiments performed under a rotating magnetic field the response experiments were conducted on rods next to a glass surface as the microgels sediment relatively fast. Of each field strength and rotation frequency a video of 3600 frames was recorded, while rotating the magnetic field. Thereby, the framerate was chosen to correlate to the rotation frequency, so that one frame corresponds to 1° of rotation of the magnetic field. With image analysis (ImageJ), the angular change of the rods was evaluated and the mean squared angular displacement was calculated. The tracking of the rotation of the microgels was performed

with the 'Analyse Particles' function of ImageJ^[31] and the Matlab routine was written for the computation and analysis of the mean squared angular displacement as described above.

Cell Culture in Anisogels: The matrix hydrogel in which the microgels were dispersed was an enzymatically cross-linked PEG hydrogel. The hydrogel was formed by the reaction between eight-arm star PEG-vinylsulfones (sPEG-VS, 20 kDa) conjugated with either a transglutaminase substrate (H-NQEQVSPLEKCG-NH₂: Q-peptide) or a free primary amine (Ac-FKGGGPGQGIWGQERCG-NH₂: K-peptide). The K-peptide possesses a matrix metalloprotease (MMP) degradable sequence GPQG↓IWGQ that enables cell-induced degradation, providing space for cells to grow inside the matrix. The enzymatic cross-linking of these conjugates was achieved by the addition of activated transglutaminase Factor XIII (FXIIIa) enzyme in presence of a calcium buffer. The protocol for the synthesis of star-PEG conjugates and activation of Factor XIII were described in detail elsewhere.^[32] The total concentration of peptide-functionalized PEG precursors in the Anisogel precursor solution was 1 wt/vol%. The two kinds of PEG-peptide conjugates were added at an equimolar concentration. The complex viscosity of the PEG precursor solution was measured to be 0.39 Pa s with a DHR3 Hybrid Rheometer (TA Instruments) using a 2° cone plate geometry with a diameter of 20 mm.

The encapsulation of pre-aligned microgel rods in a 3D hydrogel to form an Anisogel was achieved by first dispersing the microgels, along with L929 mouse fibroblast cells in a cell culture medium (RPMI 1640, Gibco). A hydrogel precursor solution was then prepared by the addition of a 10X buffer (0.1 M CaCl₂, 0.5 M Tris, 1.1 M NaCl) and star-PEG conjugates of activated factor XIII substrate peptides to this dispersion.^[32] The microgels constitute 1% of the total hydrogel volume in each of the parallelly or perpendicularly pre-programmed samples. In the condition where there were both types microgels present as well as the control condition with microgels in the absence of a magnetic field, the total microgel concentration was 2 vol.%. The cell concentration was kept at 700 cells μL⁻¹ of the hydrogel in all cases. To enable cell attachment, a solution of Fibronectin (Sigma–Aldrich) in water was added to the precursor to achieve a final protein concentration of 1 μM in the hydrogel. To this precursor, an activated enzyme Factor XIII (CSL Behring GmbH, 1250 U FXIII) was added at a concentration of 50 U mL⁻¹. The precursor solution was then mixed well to disperse the microgels and cells homogeneously and 10 μL of this solution was pipetted into each well of an Angiogenesis chamber (Ibidi) in the presence of a magnetic field (100 mT). The dispersion was then allowed to cross-link for 30 min at 37 °C in an incubator, with the magnets in place, while flipping the chamber back and forth every 5 min to prevent the settlement of microgels. After the gels were fully cross-linked, the magnets were removed and 50 μL of RPMI medium was added to each of the wells. The cells were cultured for 4 days with a media change done after every other day. After 4 days, the samples were washed three times using PBS for 30 min and then fixed using 4% paraformaldehyde for 1 h with gentle shaking. Thereafter the samples were washed three times with PBS again and cells were permeabilized by incubation with 0.1% Triton X-100 solution for 30 min. After a further washing step with PBS, the cells were blocked with 4% bovine serum albumin solution for 4 h. This was followed by the incubation with a conjugated primary antibody phalloidin 488 (Abcam 1:1000) overnight at 4 °C, to visualize the actin filaments in cells. After washing three times with PBS, the samples were incubated with DAPI (1:1000). Once again, the samples were washed three times with PBS and stored at 4 °C until imaging with a C Confocal laser scanning microscope Leica TCS SP8. Details on the setup and the consecutive image analysis can be found in the Supporting Information.

For the experiments on Anisogels using a combination of rotating and static magnetic field a 50/50 mixture of microgel with a parallel and anti-parallel orientation with a total concentration of 1 wt.% was employed. The activated enzyme Factor XIII concentration was reduced to 10 U mL⁻¹ to slow down the cross-linking kinetics. A PDMS well was made by punching out holes using a 3.5 mm biopsy punch and sticking them on an Ibidi dish bottom using autoclaved vacuum grease. 10 μL of the precursor solution was deposited inside an already rotating

magnetic field (10 rpm, 70 mT). After 4 min the engine was stopped and the gelation was let to proceed in the static field for 6 min. The Anisogel was fully cross-linked after 10 min. Three milliliters of RPMI media was added to the petri dish for culture that went on for 4 days like all other cell experiments in the manuscript. Afterward, the Anisogel was investigated via confocal microscopy.

Statistical Analysis: Details of the statistical evaluation including the programs used, sample size as well as normalization can be found in the corresponding method sections and in the Supporting Information. If not differently specified, all data are presented as mean ± standard error of the mean.

Supporting Information

Supporting Information is available from the Wiley Online Library or from the author.

Acknowledgements

D.L.B. and S.B. contributed equally to this work. The authors acknowledge the financial support of the Deutsche Forschungsgemeinschaft (DFG, German Research Foundation) in the Collaborative Research Center (CRC 985) Functional Microgels and Microgel Systems, Project B5, and the Research Training Network (RTG2415) ME3T. This research was conducted within the Max Planck School Matter to Life supported by the German Federal Ministry of Education and Research (BMBF) in collaboration with the Max Planck Society. J.J.C. acknowledges financial support from the Exploratory Research Space of RWTH Aachen University (project StUpJP_049-18 and BioTrans012). L.D.L. acknowledges support by the Leibniz Senate Competition Committee (SAW) under the Professorinnenprogramm (SAW-2017-PB62: BioMat) and the Government of Canada's New Frontiers in Research Fund (NFRF), (NFRFT-2020-00238): Mend the Gap, a Transformative Biomaterials Platform for Spinal Cord Repair. Finally, the authors thank Thiago Ito for the synthesis of the silica-coated hematite nanoparticles and Ke Ran for the TEM analysis.

Open access funding enabled and organized by Projekt DEAL.

Conflict of Interest

The authors declare no conflict of interest.

Data Availability Statement

The data that support the findings of this study are available from the corresponding author upon reasonable request.

Keywords

anisogels, anisotropic magnetic microgels, maghemite spindles, tissue engineering

Received: March 1, 2022

Revised: August 4, 2022

Published online:

[1] a) R. Fulcrand, D. Jugieu, C. Escriba, A. Bancaud, D. Bourrier, A. Boukabache, A. M. Gué, *J. Micromech. Microeng.* **2009**, 19,

- 105019; b) J. H. Jung, C. Han, S. A. Lee, J. Kim, C. Yang, *Lab Chip* **2014**, *14*, 3781.
- [2] G. Decroly, A. Toncheva, L. Blanc, J.-M. Raquez, T. Lessinnes, A. Delchambre, P. Lambert, *Actuators* **2020**, *9*, 131.
- [3] S. A. Lee, H. Lee, J. R. Pinney, E. Khialeeva, M. Bergsneider, J. W. Judy, *J. Micromech. Microeng.* **2011**, *21*, 054006.
- [4] a) U. A. Gurkan, S. Tasoglu, D. Kavaz, M. C. Demirel, U. Demirci, *Adv. Healthc. Mater.* **2012**, *1*, 149; b) S. Guven, P. Chen, F. Inci, S. Tasoglu, B. Erkmen, U. Demirci, *Trends Biotechnol.* **2015**, *33*, 269.
- [5] E. S. Place, N. D. Evans, M. M. Stevens, *Nat. Mater.* **2009**, *8*, 457.
- [6] a) G. C. Engelmayr, M. Cheng, C. J. Bettinger, J. T. Borenstein, R. Langer, L. E. Freed, *Nat. Mater.* **2008**, *7*, 1003; b) M. N. Hirt, A. Hansen, T. Eschenhagen, *Circ. Res.* **2014**, *114*, 354.
- [7] a) Y. Sun, Y. You, W. Jiang, B. Wang, Q. Wu, K. Dai, *Sci. Adv.* **2020**, *6*, eaay1422; b) M. S. Şenol, H. Özer, in *Comparative Kinesiology of the Human Body* (Eds: S. Angin, I. E. Şimşek), Academic Press, **2020**, p. 91; c) C. Madeira, A. Santhagunam, J. B. Salgueiro, J. M. S. Cabral, *Trends Biotechnol.* **2015**, *33*, 35.
- [8] J. M. Corey, D. Y. Lin, K. B. Mycek, Q. Chen, S. Samuel, E. L. Feldman, D. C. Martin, *J. Biomed. Mater. Res., Part A* **2007**, *83A*, 636.
- [9] a) I. M. Basurto, M. T. Mora, G. M. Gardner, G. J. Christ, S. R. Caliri, *Biomater. Sci.* **2021**, *9*, 4040; b) L. Agrawal, M. Saidani, L. Guillaud, M. Terenzio, *Mater. Sci. Eng., C* **2021**, *131*, 112502.
- [10] a) C. D. L. Johnson, D. Ganguly, J. M. Zuidema, T. J. Cardinal, A. M. Ziemba, K. R. Kearns, S. M. McCarthy, D. M. Thompson, G. Ramanath, D. A. Borca-Tasciuc, S. Dutz, R. J. Gilbert, *ACS Appl. Mater. Inter.* **2019**, *11*, 356; b) A. Omidinia-Anarkoli, S. Boesveld, U. Tuvshindorj, J. C. Rose, T. Haraszti, L. De Laporte, *Small* **2017**, *13*, 1702207.
- [11] a) E. J. Berns, S. Sur, L. Pan, J. E. Goldberger, S. Suresh, S. Zhang, J. A. Kessler, S. I. Stupp, *Biomaterials* **2014**, *35*, 185; b) A. Sheikhi, J. de Rutte, R. Haghniaz, O. Akouissi, A. Sohrabi, D. Di Carlo, A. Khademhosseini, *Biomaterials* **2019**, *192*, 560; c) N. F. Truong, E. Kurt, N. Tahmizyan, S. C. Lesher-Pérez, M. Chen, N. J. Darling, W. Xi, T. Segura, *Acta Biomater.* **2019**, *94*, 160.
- [12] a) J. C. Rose, M. Cámara-Torres, K. Rahimi, J. Köhler, M. Möller, L. De Laporte, *Nano Lett.* **2017**, *17*, 3782; b) J. C. Rose, D. B. Gehlen, T. Haraszti, J. Köhler, C. J. Licht, L. De Laporte, *Biomaterials* **2018**, *163*, 128.
- [13] a) J. C. Rose, L. De Laporte, *Adv. Healthc. Mater.* **2018**, *7*, 1701067; b) J. C. Rose, M. Fölster, L. Kivilip, J. L. Gerardo-Nava, E. E. Jaekel, D. B. Gehlen, W. Rohlf, L. De Laporte, *Polym. Chem.* **2020**, *11*, 496.
- [14] Y. Du, E. Lo, S. Ali, A. Khademhosseini, *Proc. Natl. Acad. Sci. U.S.A.* **2008**, *105*, 9522.
- [15] M. Karg, A. Pich, T. Hellweg, T. Hoare, L. A. Lyon, J. J. Crassous, D. Suzuki, R. A. Gumerov, S. Schneider, I. I. Potemkin, W. Richtering, *Langmuir* **2019**, *35*, 6231.
- [16] a) H. Zhang, L. Koens, E. Lauga, A. Mourran, M. Möller, *Small* **2019**, *15*, 1903379; b) Z. Özbaş, B. Özkahraman, A. Bal Öztürk, *Polym. Bull.* **2018**, *75*, 3053; c) E. S. Minina, P. A. Sánchez, C. N. Likos, S. S. Kantorovich, *J. Magn. Magn. Mater.* **2018**, *459*, 226.
- [17] A. J. Schmid, J. Dubbert, A. A. Rudov, J. S. Pedersen, P. Lindner, M. Karg, I. I. Potemkin, W. Richtering, *Sci. Rep.* **2016**, *6*, 22736.
- [18] Y. Kittel, A. J. C. Kuehne, L. De Laporte, *Adv. Healthc. Mater.* **2021**, e2101989.
- [19] a) L. P. B. Guertzoni, J. C. Rose, D. B. Gehlen, A. Jans, T. Haraszti, M. Wessling, A. J. C. Kuehne, L. De Laporte, *Small* **2019**, *15*, 1900692; b) L. P. B. Guertzoni, Y. Tsukamoto, D. B. Gehlen, D. Rommel, T. Haraszti, M. Akashi, L. De Laporte, *Biomacromolecules* **2019**, *20*, 3746.
- [20] a) D. Rommel, M. Mork, S. Vedaraman, C. Bastard, L. P. B. Guertzoni, Y. Kittel, R. Vinokur, N. Born, T. Haraszti, L. De Laporte, *Adv. Sci.* **2022**, n/a, 2103554; b) T. H. Qazi, J. Wu, V. G. Muir, S. Weintraub, S. E. Gullbrand, D. Lee, D. Issadore, J. A. Burdick, *Adv. Mater.* **2022**, *34*, 2109194; c) A. C. Daly, L. Riley, T. Segura, J. A. Burdick, *Nat. Rev. Mater.* **2020**, *5*, 20; d) D. R. Griffin, W. M. Weaver, P. O. Scumpia, D. Di Carlo, T. Segura, *Nat. Mater.* **2015**, *14*, 737.
- [21] J. C. Rose, D. B. Gehlen, A. Omidinia-Anarkoli, M. Fölster, T. Haraszti, E. E. Jaekel, L. De Laporte, *Adv. Healthc. Mater.* **2020**, *9*, 2000886.
- [22] J. Kim, J. R. Staunton, K. Tanner, *Adv. Mater.* **2016**, *28*, 132.
- [23] V. Malik, A. Pal, O. Pravaz, J. J. Crassous, S. Granville, B. Grobety, A. M. Hirt, H. Dietsch, P. Schurtenberger, *Nanoscale* **2017**, *9*, 14405.
- [24] I. Martchenko, H. Dietsch, C. Moitzi, P. Schurtenberger, *J. Phys. Chem. B* **2011**, *115*, 14838.
- [25] Z. Li, C. Qian, W. Xu, C. Zhu, Y. Yin, *Sci. Adv.* **2021**, *7*, eab11289.
- [26] K. G. Kornev, Y. Gu, P. Aprelev, A. Tokarev, in *Magnetic Characterization Techniques for Nanomaterials* (Ed: C. S. S. R. Kumar), Springer, Berlin, Heidelberg **2017**.
- [27] B. Frka-Petesic, K. Erglis, J. F. Berret, A. Cebers, V. Dupuis, J. Fresnais, O. Sandre, R. Perzynski, *J. Magn. Magn. Mater.* **2011**, *323*, 1309.
- [28] D. Hoffelner, M. Kundt, A. M. Schmidt, E. Kentzinger, P. Bender, S. Disch, *Faraday Discuss.* **2015**, *181*, 449.
- [29] a) H. L. Karlsson, P. Cronholm, J. Gustafsson, L. Möller, *Chem. Res. Toxicol.* **2008**, *21*, 1726; b) H. L. Karlsson, J. Gustafsson, P. Cronholm, L. Möller, *Toxicol. Lett.* **2009**, *188*, 112; c) N. Singh, G. J. S. Jenkins, R. Asadi, S. H. Doak, *Nano Rev.* **2010**, *1*, 5358.
- [30] L. Wang, Z. Meng, Y. Chen, Y. Zheng, *Adv. Intell. Syst.* **2021**, *3*, 2000267.
- [31] M. Abramoff, P. Magalhães, S. J. Ram, *Biophotonics Int.* **2003**, *11*, 36.
- [32] C. Licht, J. C. Rose, A. O. Anarkoli, D. Blondel, M. Roccio, T. Haraszti, D. B. Gehlen, J. A. Hubbell, M. P. Lutolf, L. De Laporte, *Biomacromolecules* **2019**, *20*, 4075.